MAGNETIC AND ELECTRICAL PROPERTIES OF H13 TOOL STEEL BY BOUND METAL DEPOSITION 3D PRINTING: ANNEALED AND NON-ANNEALED

Le Hoang Trong Minh^{©1}, Do Qui Duyen^{©1,*}, Ngo Chi Vinh^{©2}, Nguyen Quoc Hung^{©2}, Le Vu Phuong Trinh^{©3}

¹Faculty of Engineering, Vietnamese-German University, Ben Cat City, Vietnam
²Institute of Engineering, HUTECH University, Ho Chi Minh City, Vietnam
³Faculty of Electrical and Electronics Engineering, Dalat College, Lam Dong Province, Vietnam
*E-mail: dq.duyen@vgu.edu.vn

Received: 14 January 2025 / Revised: 15 April 2025 / Accepted: 08 May 2025 Published online: 30 June 2025

Abstract. In recent years, a new additive manufacturing process called bound metal deposition has emerged and advanced dramatically. While most studies have concentrated mainly on the mechanical properties of 17-4PH stainless steel, with some focus on tool steels, there remains a gap in studies exploring a wider variety of materials and other applications. This study aims to address this by using another type of steel, namely H13 tool steel. The material is employed to form 3D-printed samples through the bound metal deposition process. Material characterizations of magnetic and electrical properties are subsequently performed on the printed samples. In addition, the impact of a thermal annealing post-process is studied to better understand its effects on the material properties. Underlying mechanisms responsible for changes in material properties are proposed to provide valuable insights into different treatments that influence the behavior of the investigated materials. Additional samples of conventional hot-rolled SKD61 tool steel will also be measured and compared with the 3D-printed samples. The findings of this research significantly expand the potential applications of 3D-printed steel materials, particularly in fields that rely on magnetic and electrical characteristics. By exploring a broader range of steels and processing techniques, this study enhances understanding of the capabilities of additive manufacturing in producing materials with diverse functional properties.

Keywords: bound metal deposition 3D printing, magnetic properties, electrical properties, tool steels, H13 tool steel, SKD61 tool steel.

1. INTRODUCTION

Additive Manufacturing (AM), also known as Three-Dimensional (3D) printing, is the process of creating 3D objects by adding material layer by layer based on parametric 3D models from computer-aided design (CAD) software. Theoretically, AM has huge advantages in manufacturing objects with high geometric complexity and reducing the amount of wasted material, which is impossible to achieve by traditional manufacturing methods, also known as subtractive manufacturing [1]. Ever since it was patented in 1979, AM has developed more than 20 different techniques, and new ones are still emerging [2]. With the variety of methods, AM has been widely used for rapid prototyping or small-batch production, making it easy to adapt to industries such as aerospace [3], automotive [4], medical [5,6], or construction [7]. Additionally, different approaches provide AM with the ability to work with a variety of materials, from plastics to metals. Among the emerging techniques, Fused Deposition Modeling (FDM) is noted as the most prevalent one, as it is fast to produce, easy to access, and efficient in cost [8]. The process can simply be described as the creation of an object by extruding material layer by layer via a heated nozzle onto a heated bed. Recently, research related to FDM has focused on developing polymers and polymer composites to use in the FDM process. Besides FDM, other methods have been developed to produce high-quality metal components. The prominent metal AM technologies include powder bed fusion processes such as Selective Laser Sintering (SLS) and Electron Beam Melting (EBM). These processes generate a heat source (laser or electron beam) to sinter or melt the metal powder layer by layer to form the final metal part. The latest developed technology for metal AM is Bound Metal Deposition (BMD) [9,10]. This process is developed based on FDM as it extrudes metal rods instead of plastic filaments. The metal rod is a mixture of metal powder held together by a proportion of polymer binder and coated with wax. The process involves the extrusion of the metal rod layer by layer based on geometry through a heated nozzle to realize the part. The realized part later goes through the required debinding and sintering processes to remove the polymer binder and sinter the metal component. As a result, a densified solid part is obtained, whose mechanical properties are competitive compared to metal parts fabricated by conventional manufacturing methods [11].

The magnetic property of a material plays a crucial role in machinery, as not only is it fundamental to the operation of many machines and equipment, but it also has a direct impact on their performance, application, and evolution. Achieving desired magnetic properties in 3D-printed metal parts has been very challenging due to the limited material options, the high precision required in microstructure [11], changes in material properties due to process heat, and more. From another perspective, recent AM technology has shown remarkable progress, opening up the possibility for manufacturing parts with desired magnetism.

The electrical properties of materials refer to their ability to respond to electric fields and electric currents, including basic properties related to electrical conductivity, insulation, and the storage of electrical energy. These properties play an important role in defining the efficiency, application, and development of all electrical equipment. Similar to magnetic properties, there are great challenges and possibilities for 3D printing metal parts to achieve the desired electrical specifications [12].

In this study, H13 tool steel parts were fabricated using BMD technology, and SKD61 tool steel parts were fabricated using conventional manufacturing technology. The parts underwent two different post-processes, which are with and without annealing. The magnetic and electrical properties of each material were measured and compared with each other in the same and different processes. The underlying mechanisms behind the observed differences were analyzed, and the results suggest the impact of different postprocessing on the magnetic and electrical properties of 3D-printed parts.

2. MATERIALS AND METHODS

2.1. Material

H13 tool steel spool (Markforged, USA) is a chromium-molybdenum hot work steel that is widely used in hot work and cold work tooling applications. Table 1 shows the material composition of the investigated H13 tool steel spool. It is known for its excellent combination of toughness, wear resistance, and resistance to thermal fatigue.

Table 1. The material composition of H13 tool steel

Cr	Mo	Si	V	С	Mn	P	S	Fe
4.7–5.5	1.3–1.7	0.8-1.2	0.8-1.2	0.3-0.45	0.2-0.5	0.03 max	0.03 max	Balance

The metal ceramic support material spool (Markforged, USA) is used as the base and support layer for other metal materials in the BMD process.

SKD61 tool steel (ASSAB Vietnam Co., Ltd, Vietnam) is a high-performance hot work steel renowned for its exceptional combination of toughness, wear resistance, and heat resistance. Its composition is shown in Table 2.

Table 2. The material composition of SKD61 tool steel

Cr	Mo	Si	V	С	Mn	P	S	Fe
4.8–5.5	1.0-1.5	0.8–1.2	0.8–1.15	0.35-0.42	0.25-0.3	0.02 max	0.02 max	Balance

SKD61 tool steel is chosen to compare with H13 as they are alloy tool steels with equivalent steel standards. The equivalent standards are shown in Table 3.

China	Russia	Japan	USA	British	Germany	France	ISO
GB1299-85	GOST 5950-73	JIS G4401-83	ASTM 681-94	BS 4659-89	DIN 17350-80	NF A35-590-92	4957
4Cr5MoSiV1	4KH5MF1S	SKD61	H13	BH13	X40CrMoV5-1	X40CrMoV5	40CrMoV5

Table 3. H13 tool steel equivalent standards [13]

2.2. Method

The samples were prepared using a Markforged Metal X printer (Markforged, USA) specialized for BMD technology. The Markforged Metal X printer includes two main chambers: the material spools chamber and the printing bed chamber. The material chamber can be loaded with two different types of spools (ceramic and metal). The spools are directly connected to the heated nozzle, which can actively extrude and retract between the two filaments. The printing chamber includes the printing bed and the nozzle, which are similar to those in FDM technology. In addition to the printing chamber, a printing sheet is placed on the bed, which later supports the removal of the work pieces. The sample was designed in a cylindrical shape with a dimension of 10 mm diameter and 50 mm length (Ø10 mm × 50 mm) using NX design software. The model was exported to an STL file and uploaded to the Markforged Cloud site for the slicing process. The printing parameter was set at 100% infill and 0.125 mm layer thickness. The overall BMD process flow for producing experimental samples is illustrated in Fig. 1. To prepare for the printing process, some pre-printing setup must be done. One roll of metal spool (H13) and one roll of ceramic spool (Metal Ceramic Support Material) need to be loaded in a heated chamber. In the printing chamber, a printing sheet needs to be vacuumed and pressed in order to stick to the printing bed. When the pre-printing setup was completed, the printing process could be started via the Markforged Cloud site and lasted for 4 hours. After the printing process was finished, samples needed to be gently removed and subjected to post-processing, which included debinding and sintering. A comparison of H13 samples at different processing stages is shown in Fig. 2.

The debinding process is executed using a Markforged Wash-1 station (Markforged, USA), which is used to remove binding material (polymer) from printed parts produced by the Markforged Metal X printer. Printed parts were placed in a basket and dipped into the immersion chamber filled with solvent (Opteon™ SF79). The solvent was heated in the boiling chamber at 55 °C and circulated to the immersion chamber. The debinding process took 12 hours to chemically remove the binding material from the printed parts and an additional 5 hours to dry in the drying chamber before the sintering process.

The sintering process was executed using the Markforged Sinter-1 station (Markforged, USA). The washed and dried parts were placed on a ceramic plate in the same orientation as during the printing process. The plate was then slid into the furnace tube until it reached the end. The radiation shield was also slid into the furnace tube until the end. When this was done, the furnace inlet door was closed and secured.

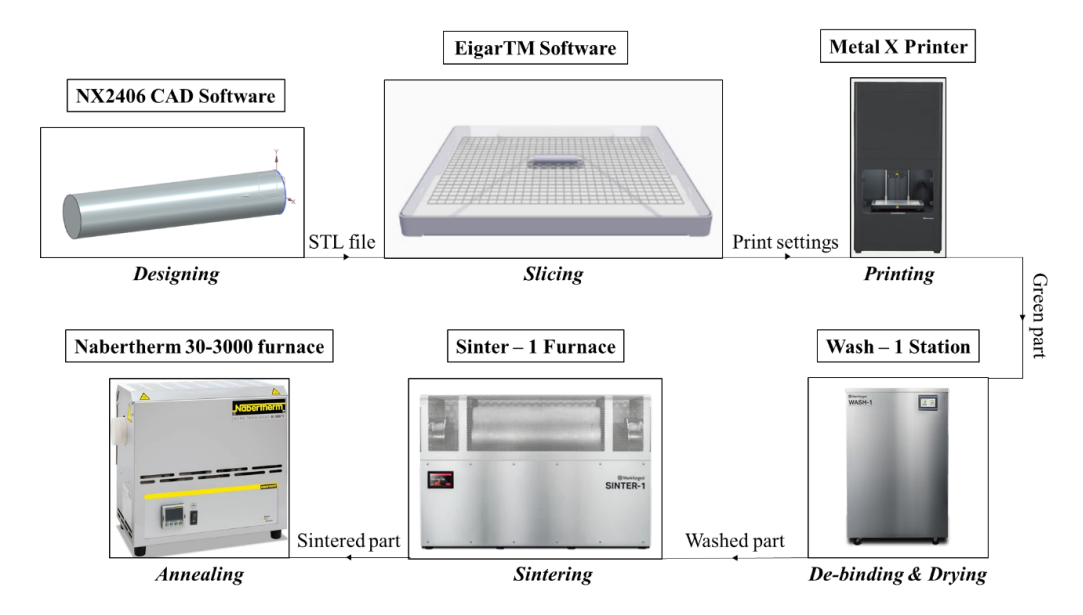


Fig. 1. BMD process for experimental samples



Fig. 2. Comparison of H13 samples at different stages

Finally, the supply of mixed gas consisting of 95% H₂ and 5% Ar (Messer Vietnam Industrial Gases Co., Ltd, Vietnam) needed to be checked before the sintering process started. The sintering process took 12 hours to finish. After the sintering process, one part of each material underwent the annealing process using a Nabertherm 30-3000 furnace (Nabertherm Inc., USA). The sample was placed inside the furnace and went through a

6-hour annealing process. The process included 1 hour of heating to 1000 $^{\circ}$ C and 5 hours of slow cooling at a rate of 200 $^{\circ}$ C per hour.

2.3. Characterization

The magnetic properties of 3D-printed H13 tool steel and conventional hot-rolled SKD61 tool steel at two different stages (pre-annealing and annealing) were measured using a copper coil. The copper coil was wound with 400 turns of 0.25-mm copper wire around a plastic spool. The samples were inserted in the middle of the coil before the measurement. The process of measuring the magnetic field is shown in Fig. 3. Measurements were taken at different values of the current source from 0.1 to 2.5 A with a step of 0.1 A. A magnetic sensor was placed close to the coil to measure the magnetic field values. Each sample was measured and the values were recorded. The recorded data were used to demonstrate the relationship between the magnetic field and different input currents.

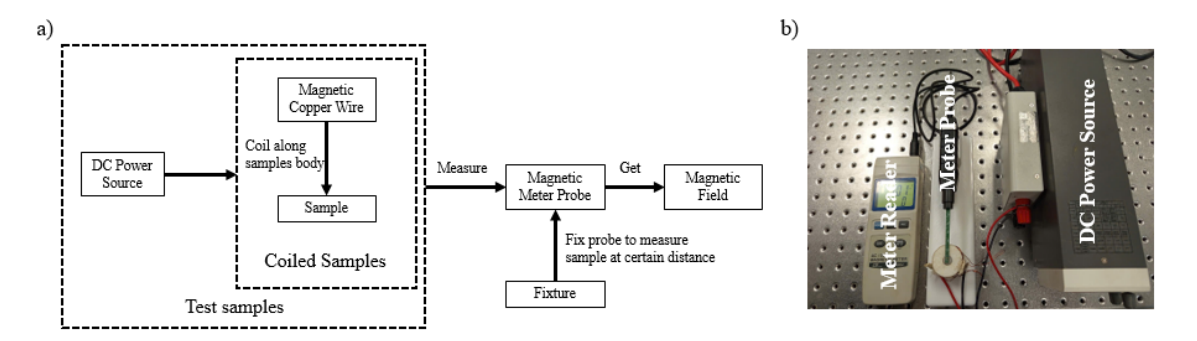


Fig. 3. (a) Arrangement diagram of experimental equipment, and (b) measurement setup for magnetic property



Fig. 4. Measurement setup of electric property on APX-4C Model Probe Station

The electrical properties of the 3D-printed H13 tool steel samples and conventional hot-rolled SKD61 samples at two different stages (pre-annealing and annealing) were measured using the APX-4C Model Probe Station. The setup for the current measurement is shown in Fig. 4. The distance between the two probe heads was fixed at 4 mm. The current was measured at different voltages from -0.1 to 0.1 V with a step of 0.01 V generated by the station.

3. RESULT AND DISCUSSION

3.1. Magnetic properties

Fig. 5 shows the relationship between the magnetic field and different current values from 0.1 A to 2.5 A for four different samples from two different materials (3D-printed H13 tool steel and hot-rolled SKD61 stainless steel) at two different stages (before and after the annealing process). The data for Fig. 5 are given in Table 4. At current values below 0.7 A, the magnetic field values for all the samples were nearly the same except for the sample of 3D-printed H13 tool steel pre-annealing, which was remarkably higher than the other samples. However, as the current increased above 0.7 A, the 3D-printed H13 tool steel pre-annealing sample showed a smaller slope compared to the other samples. Also, as the current increased further, the differences in the magnetic field among the samples became more distinct. At low current values, the magnetic field was not fully formed, which made the effects of sample properties such as porosity, grain size, and surface roughness on the value of the magnetic field unclear [11]. On the other hand, as the

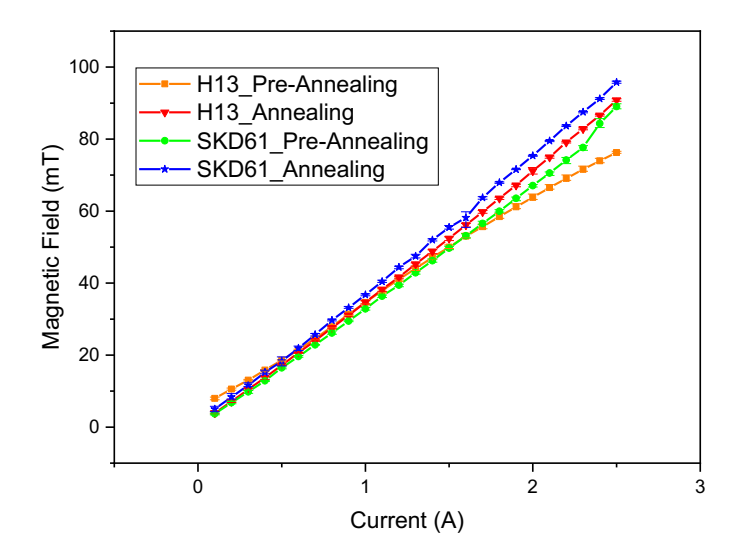


Fig. 5. Graph of current versus magnetic field for 3D-printed H13 tool steel and hot-rolled SKD61 tool steel at two different stages: Pre-annealing and annealing

current increased, the magnetic field reached a fully formed and saturated stage [11]. At this stage, any small differences in sample properties could have a clear impact on the overall value of the magnetic field. At the maximum recorded current value of 2.5 A, the magnetic field values of the 3D-printed H13 and hot-rolled SKD61 stainless steel samples before and after annealing were 76.27 mT, 90.83 mT, 89.03 mT, and 95.8 mT, respectively.

Table 4. Data table of recorded magnetic values of H13 and SKD61 tool steels at two different stages: Pre-annealing and annealing

Current		Pre-Annea	ling	H13 Annealing			SKD61 Pre-Annealing			SKD61 Annealing		
Current	Average	Tor (+)	Tol (-)	Average	Tor (+)	Tol (-)	Average	Tor (+)	Tol (-)	Average	Tor (+)	Tol (-)
0.1	7.98333	0.36667	0.38333	3.95	0.45	0.25	3.7	0.2	0.3	5.03333	0.76667	0.73333
0.2	10.58333	0.26667	0.33333	7.11667	0.38333	0.26667	6.8	0.4	0.3	8.36667	0.93333	0.56667
0.3	13.03333	0.21667	0.18333	10.45	0.2	0.25	9.8	0.4	0.4	11.63333	0.66667	0.33333
0.4	15.83333	0.16667	0.23333	13.75	0.25	0.5	12.866 67	0.13333	0.16667	15.2	0.6	0.4
0.5	18.61667	0.13333	0.26667	17.21667	0.03333	0.01667	16.46667	0.23333	0.266 67	18.33333	1.16667	1.33333
0.6	21.46667	0.18333	0.21667	20.65	0.1	0.15	19.6	0.3	0.2	21.93333	0.56667	0.63333
0.7	24.6	0.35	0.35	24.01667	0.18333	0.16667	22.866 67	0.0333	0.06667	25.7	0.3	0.4
0.8	27.9	0.3	0.35	27.566 67	0.33333	0.26667	26.133 33	0.56667	0.33333	29.66667	0.33333	0.16667
0.9	31.38333	0.41667	0.33333	31.03333	0.36667	0.33333	29.466 67	0.23333	0.16667	33.16667	0.33333	0.16667
1	34.65	0.4	0.45	34.66667	0.53333	0.46667	32.866 67	0.33333	0.366 67	36.76667	0.23333	0.26667
1.1	37.9	0.55	0.6	38.266 67	0.43333	0.56667	36.366 67	0.33333	0.366 67	40.43333	0.36667	0.23333
1.2	41.05	0.65	0.5	41.66667	0.23333	0.46667	39.466 67	0.23333	0.46667	44.4	0.3	0.4
1.3	44.05	0.7	0.55	45.28333	0.31667	0.58333	42.866 67	0.33333	0.366 67	47.5	0.5	0.5
1.4	47.13333	0.76667	0.48333	48.85	0.4	0.65	46.233 33	0.46667	0.43333	52	0.3	0.3
1.5	50.01667	0.58333	0.41667	52.41667	0.43333	0.61667	49.733 33	0.46667	0.43333	55.5	0.5	0.5
1.6	53.03333	0.81667	0.43333	56.13333	0.41667	0.53333	53.133 33	0.56667	0.63333	58.16667	1.63333	2.666 67
1.7	55.66667	0.73333	0.56667	59.76667	0.38333	0.36667	56.566 67	0.63333	0.366 67	63.73333	0.26667	0.43333
1.8	58.46667	0.88333	0.46667	63.53333	0.31667	0.28333	59.96667	0.43333	0.266 67	67.9	0.2	0.2
1.9	61.16667	0.88333	0.46667	67.16667	0.28333	0.41667	63.566 67	0.33333	0.66667	71.56667	0.13333	0.06667
2	63.78333	0.96667	0.53333	71.16667	0.93333	0.86667	67.066 67	0.33333	0.366 67	75.4	0.1	0.2
2.1	66.53333	0.81667	0.43333	74.96667	0.33333	0.26667	70.566 67	0.33333	0.66667	79.5	0.1	0.2
2.2	69.06667	0.98333	0.51667	79.13333	0.16667	0.23333	74.166 67	0.73333	0.966 67	83.66667	0.23333	0.16667
2.3	71.58333	0.91667	0.53333	82.86667	0.23333	0.26667	77.666 67	0.53333	0.766 67	87.5	0.2	0.2
2.4	73.95	0.7	0.5	86.6	0.2	0.2	84.333 33	1.366 67	1.133 33	91.2	0.3	0.2
2.5	76.26667	0.33333	0.21667	90.83333	0.36667	0.33333	89.03333	0.76667	0.633 33	95.8	0.3	0.3

Compared to the two materials, the hot-rolled SKD61 stainless steel samples had magnetic field values at a current of 2.5 A at two different stages (before and after annealing) that were higher than those of the 3D-printed H13 samples by approximately 16.74% and 5.47%, respectively. The reason for this difference could be attributed to surface roughness and porosity. The 3D-printed H13 material using the BMD technique had a visible layer thickness (0.125 mm), which resulted in a rough surface of the model. The rough surface could hinder or trap the natural direction of magnetic domains and result in a weakening of the material's magnetic field [14, 15]. Porosity was an unavoidable defect inside the structure of the 3D-printed part, as it was challenging to control the

presence of voids after the sintering and annealing processes when the binding material was removed and the metal part had to restructure. This defect affected the magnetic field similarly to surface roughness [16].

Compared between the two different stages, hot-rolled SKD61 stainless steel samples and 3D-printed H13 tool steel samples had magnetic field values at a current of 2.5 A that increased by 7.6% and 19.1% after annealing, respectively. The improvement in magnetic field values came mostly from the reduction of porosity as the grain size improved during the annealing process. Additionally, comparing the two materials at each stage, the 3Dprinted H13 tool steel samples had lower magnetic field values compared to the hotrolled SKD61 tool steel by 16.7% and 5.46% for pre-annealing and annealing, respectively.

The gap in improvement rate between the two materials shows the potential for 3Dprinted H13 tool steel for practical applications in Vietnam. To reduce the gap between 3D-printed H13 tool steel and hot-rolled SKD61 tool steel, the researchers plan to investigate the optimal temperature for the annealing process in order to improve the grain size and reduce porosity inside the material. Additionally, polishing the 3D-printed samples to improve surface roughness or changing the sample printing orientation could be considered effective approaches to improve magnetic properties.

3.2. Electrical properties

The data for Figs. 6(a) and 6(b) are given in Table 5. Fig. 6(a) illustrates the response of current resistance to the change in supply voltage from -0.1 V to 0.1 V for the two materials before the annealing process. The values of current resistance for the two materials could be considered similar, with a very small gap of 0.061 Ω on average before the annealing process. This gap can be explained by the electrical resistivity (ρ) of each material. The relationship between resistance (Ω) and electrical resistivity is shown in Eq. (1). As the two materials have similarities in composition, the electrical resistivity can be assumed to be nearly the same, which may be directly measured in future research. The length of the two samples is the same. In contrast, the cross-section of the SKD61 sample is a circle, while the cross-section of the H13 sample with the same diameter is not a full circle due to the nature of 3D printing, which creates a small difference in the cross-sectional area of the two samples. Because of that difference, a gap in the resistance of the two samples is observed. Additionally, the tolerance for the current resistance of the two materials was small, at -2.1% to 2.2% and -2.8% to 1.3% for H13 and SKD61, respectively. These values showed high consistency in the current resistance of the two materials.

Eq. (1) is presented below [17]

$$R = \rho \frac{L}{A},\tag{1}$$

where *R* is resistance (Ω) , ρ is electrical resistivity $(\Omega \cdot m)$, *L* is the length of the sample (m), and *A* is the area of the cross-section of the sample (m^2) .

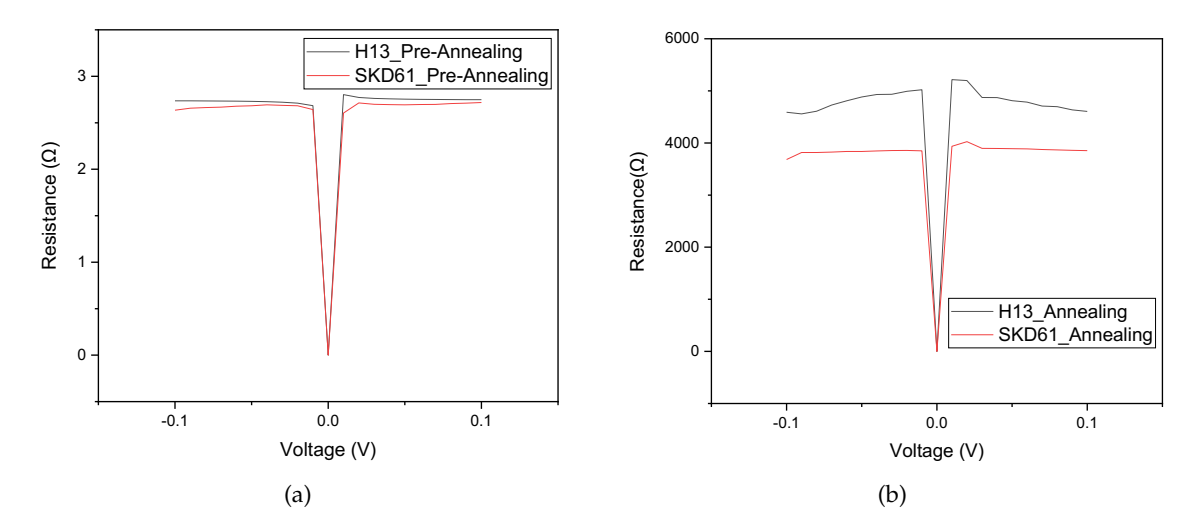


Fig. 6. Graph of voltage versus resistance for 3D-printed H13 tool steel and hot-rolled SKD61 tool steel at: (a) pre-annealing stage and (b) annealing stage

Fig. 6(b) illustrates the response of current resistance to the change in supply voltage from -0.1 V to 0.1 V for the two materials after the annealing process. The values of current resistance for the two materials increased significantly compared to the prior stage, with the H13 sample showing an average resistance approximately 962 Ω higher than the SKD61 sample after annealing. As a result, the hot-rolled SKD61 tool steel exhibited better electrical conductivity compared to the 3D-printed H13 tool steel. The increase in resistivity can be explained by the presence of metal carbides, which have higher electrical resistivity than pure metal, in the two samples after the annealing process-around 2–6% as shown in Yang's study [18]. The remarkable gap between the resistance values of the two samples can be attributed to the higher density of defects in the H13 sample compared to the SKD61 sample after annealing, which results in a larger total cross-sectional area and lower resistance for the SKD61 sample, based on the theory in Eq. (1). According to Wang's experiment, the H13 sample from the metal 3D printing approach has a higher density of porosities compared to the sample from the conventional approach [19]. The research from Ibrahim's group further reinforces the relationship between high porosity density and high resistivity [20]. The group also mentions that non-uniform void distribution produced by partial sintering causes more tortuous conduction paths, which affect the conductivity of the sample and increase the resistivity of the H13 sample [20]. The tolerances for the current resistance of the two materials were -5.5% to 8.18% and -4.6% to 4.26% for the H13 and SKD61 samples, respectively. These values show the fluctuation in the conductivity properties of the two materials.

Table 5. Data table of recorded electrical values of H13 and SKD61 tool steels at two different stages: Pre-annealing and annealing

Voltage	Pre-An	nealing	Annealing			
voltage	H13	SKD61	H13	SKD61		
-0.1	2.736 18	2.635 68	4589.6	3682.27		
-0.09	2.735 57	2.6566	4557.72	3817.99		
-0.08	2.734 53	2.6633	4609.81	3816.97		
-0.07	2.733 55	2.66784	4729.06	3824.25		
-0.06	2.732 03	2.67881	4809.1	3836.02		
-0.05	2.729 87	2.68285	4883.05	3837.78		
-0.04	2.72683	2.69297	4929.46	3847.17		
-0.03	2.721 35	2.68731	4935.2	3854.13		
-0.02	2.711 09	2.68237	4991.87	3857.2		
-0.01	2.684 42	2.642 06	5020.58	3848.24		
0	0	0	0	0		
0.01	2.8033	2.604 57	5215.97	3936.57		
0.02	2.77274	2.71373	5198.73	4024.71		
0.03	2.762 35	2.699 01	4872.73	3897.13		
0.04	2.757 36	2.69534	4871.32	3895.35		
0.05	2.754 16	2.69333	4811.9	3890.85		
0.06	2.7523	2.69674	4784.13	3885.59		
0.07	2.75073	2.69732	4707.88	3875.11		
0.08	2.749 59	2.70606	4697.62	3865.84		
0.09	2.748 88	2.71099	4635.37	3858.89		
0.1	2.748 14	2.71811	4606.45	3852.45		

4. CONCLUSION

The magnetic and electrical properties of the 3D-printed H13 tool steel samples at two different stages were measured and compared to those of conventional hot-rolled SKD61 tool steel samples. Through the recorded values, the study uncovered the differences in magnetic behavior and current resistance characteristics of the investigated materials. The mechanisms responsible for the magnetic behaviors were thoroughly analyzed, providing valuable insights into the relationship between BMD process parameters and the resulting magnetic performance of H13 tool steel. Based on these insights, ideas for improvements and optimizations of 3D-printed H13 tool steel for magnetic applications were proposed by the researchers. This study highlights the potential of employing 3D-printed H13 tool steel in a wide range of magnetic applications, especially as a replacement for magnetic materials like conventional hot-rolled SKD61 tool steel. The relation between the magnetic field and current resistance after the annealing stage can

be observed: as the magnetic field increases, the current resistance increases as well. This research also expands the applications of additive manufacturing technologies, especially in the field of advanced magnetic and electrical materials and devices.

DECLARATION OF COMPETING INTEREST

The authors declare that they have no known competing financial interests or personal relationships that could have appeared to influence the work reported in this paper.

ACKNOWLEDGMENT

This work was supported by research funds from a 2024 VGU-level project under the grant No. DTCS2024-002.

REFERENCES

- [1] K. V. Wong and A. Hernandez. A review of additive manufacturing. *International Scholarly Research Notices*, **2012**, (2012), pp. 1–10. https://doi.org/10.5402/2012/208760.
- [2] J. Fan, L. Zhang, S. Wei, Z. Zhang, S.-K. Choi, B. Song, and Y. Shi. A review of additive manufacturing of metamaterials and developing trends. *Materials Today*, **50**, (2021), pp. 303–328. https://doi.org/10.1016/j.mattod.2021.04.019.
- [3] B. Blakey-Milner, P. Gradl, G. Snedden, M. Brooks, J. Pitot, E. Lopez, M. Leary, F. Berto, and A. du Plessis. Metal additive manufacturing in aerospace: A review. *Materials & Design*, **209**, (2021). https://doi.org/10.1016/j.matdes.2021.110008.
- [4] J. C. Vasco. Additive manufacturing for the automotive industry. In *Additive Manufacturing*, Elsevier, (2021), pp. 505–530. https://doi.org/10.1016/b978-0-12-818411-0.00010-0.
- [5] C. Culmone, G. Smit, and P. Breedveld. Additive manufacturing of medical instruments: A state-of-the-art review. *Additive Manufacturing*, **27**, (2019), pp. 461–473. https://doi.org/10.1016/j.addma.2019.03.015.
- [6] C.-V. Ngo, Q. A. Nguyen, N. Le, N. L. Le, and Q. H. Nguyen. Fabrication of airy, light-weight polymer below-elbow cast by a combination of 3D scanning and 3D printing. In *Advances in Asian Mechanism and Machine Science: Proceedings of IFToMM Asian MMS* 2021, Springer International Publishing, Vol. 6, (2022), pp. 628–637. https://doi.org/10.1007/978-3-030-91892-7_60.
- [7] D. Delgado Camacho, P. Clayton, W. J. O'Brien, C. Seepersad, M. Juenger, R. Ferron, and S. Salamone. Applications of additive manufacturing in the construction industry A forward-looking review. *Automation in Construction*, 89, (2018), pp. 110–119. https://doi.org/10.1016/j.autcon.2017.12.031.
- [8] K. Rajan, M. Samykano, K. Kadirgama, W. S. W. Harun, and M. M. Rahman. Fused deposition modeling: process, materials, parameters, properties, and applications. *The International Journal of Advanced Manufacturing Technology*, **120**, (2022), pp. 1531–1570. https://doi.org/10.1007/s00170-022-08860-7.
- [9] B. Iacopo, D. P. Valerio, M. Tommaso, P. Massimiliano, and V. Alessio. Environmental impacts assessment of bound metal deposition 3D printing process for stainless steel. *Procedia CIRP*, **105**, (2022), pp. 386–391. https://doi.org/10.1016/j.procir.2022.02.064.

- [10] D. H. M. Hieu, D. O. Duyen, N. P. Tai, N. V. Thang, N. C. Vinh, and N. O. Hung. Crystal structure and mechanical properties of 3D printing parts using bound powder deposition method. In Modern Mechanics and Applications: Select Proceedings of ICOMMA 2020, Springer Singapore, (2021), pp. 54–62. https://doi.org/10.1007/978-981-16-3239-6_4.
- [11] X. Wei, M.-L. Jin, H. Yang, X.-X. Wang, Y.-Z. Long, and Z. Chen. Advances in 3D printing of magnetic materials: Fabrication, properties, and their applications. Journal of Advanced *Ceramics*, **11**, (2022), pp. 665–701. https://doi.org/10.1007/s40145-022-0567-5.
- [12] Z. E. Vandervort, N. J. Lockhart, and A. S. Hollinger. 3D printing conductive filament for fuel cell bipolar plates. In ECS Meeting MA2024-02, The Electrochemical Society, Vol. MA2024-02, (2024), pp. 3249–3249. https://doi.org/10.1149/ma2024-02463249mtgabs.
- N. Trieu. Steel standard equipvalent. Accessed (2018).https://dohaco.com.vn/blogs/kien-thuc-chuyen-nganh/bo-tieu-chuan-thep-tuongduong-steel-standard-equipvalent.
- [14] D. Aurongzeb, K. B. Ram, and L. Menon. Influence of surface/interface roughness and grain size on magnetic property of Fe/Co bilayer. Applied Physics Letters, 87, (2005). https://doi.org/10.1063/1.2119427.
- [15] Y.-P. Zhao, R. M. Gamache, G.-C. Wang, T.-M. Lu, G. Palasantzas, and J. T. M. De Hosson. Effect of surface roughness on magnetic domain wall thickness, domain size, and coercivity. Journal of Applied Physics, 89, (2001), pp. 1325–1330. https://doi.org/10.1063/1.1331065.
- [16] F. Ternero, L. G. Rosa, P. Urban, J. M. Montes, and F. G. Cuevas. Influence of the total porosity on the properties of sintered materials—A review. Metals, 11, (2021). https://doi.org/10.3390/met11050730.
- [17] Y. Singh. Electrical resistivity measurements: A review. International Journal of Modern Physics: Conference Series, 22, (2013), pp. 745–756. https://doi.org/10.1142/s2010194513010970.
- [18] Y. Guanghua, H. Xinmin, W. Yanqing, Q. Xingguo, Y. Ming, C. Zuoming, and J. Kang. Effects of heat treatment on mechanical properties of H13 steel. Metal Science and Heat Treatment, 52, (2010), pp. 393–395. https://doi.org/10.1007/s11041-010-9288-4.
- [19] M. Wang, Y. Wu, Q. Wei, and Y. Shi. Thermal fatigue properties of H13 hot-work tool steels processed by selective laser melting. Metals, https://doi.org/10.3390/met10010116.
- [20] K. A. Ibrahim, B. Wu, and N. P. Brandon. Electrical conductivity and porosity in stainless steel 316L scaffolds for electrochemical devices fabricated using selective laser sintering. Materials & Design, 106, (2016), pp. 51–59. https://doi.org/10.1016/j.matdes.2016.05.096.